Optics Letters

Direct generation of spatial quadripartite continuous variable entanglement in an optical parametric oscillator

Kui Liu,[1,2] Jun Guo,[1,2] Chunxiao Cai,[1,2] Junxiang Zhang,[1,2] and Jiangrui Gao[1,2,*]

[1]State Key Laboratory of Quantum Optics and Quantum Optics Devices, Institute of Opto-Electronics, Shanxi University, Taiyuan, Shanxi 030006, China
[2]Collaborative Innovation Center of Extreme Optics, Shanxi University, Taiyuan, Shanxi 030006, China
*Corresponding author: jrgao@sxu.edu.cn

Received 4 July 2016; revised 27 September 2016; accepted 4 October 2016; posted 4 October 2016 (Doc. ID 269347); published 4 November 2016

Multipartite entanglement is used for quantum information applications, such as building multipartite quantum communications. Generally, generation of multipartite entanglement is based on a complex beam-splitter network. Here, based on the spatial freedom of light, we experimentally demonstrated spatial quadripartite continuous variable entanglement among first-order Hermite–Gaussian modes using a single type II optical parametric oscillator operating below threshold with an $HG_{02}^{45^\circ}$ pump beam. The entanglement can be scalable for larger numbers of spatial modes by changing the spatial profile of the pump beam. In addition, spatial multipartite entanglement will be useful for future spatial multichannel quantum information applications.

OCIS codes: (270.6570) Squeezed states; (190.4410) Nonlinear optics, parametric processes.

http://dx.doi.org/10.1364/OL.41.005178

Quantum entanglement [1] is not only a fundamental issue in physics but also plays a significant role in quantum information processing [2,3]. Recently, much research has been devoted to sources of multipartite entanglement, which is the key ingredient for quantum communication and computation.

Based on an optical system, schemes for generating multipartite entangled states are commonly achieved with a linear optical transformation of a beam-splitter network [3,4]. Recently, several impressive demonstrations of multi-partite entanglement have been shown, such as 8-photon cluster states [5] and an 8-beam state [6]. However, a practical source is not only scalable, but can also be compact, even when the number of modes is very large. Recently, larger continuous variable (CV) multipartite entanglement using an optical parametric oscillator (OPO) was demonstrated in the frequency domain [7,8] and ultra-larger-scale cluster states of more than 10,000 modes were reported in time domain [9].

Spatial freedom of light is an effective approach to scale the number of entangled states. Many great achievements, especially in the discrete variable (DV) domain, have promoted the development of quantum information [3]. Parallel to the DV domain, CV spatial mode entanglement has been a hot topic of investigation because of the applications in quantum information [10] and quantum metrology [11,12]. An eight-mode Greenberger-Horne-Zeilinger (GHZ) CV entangled state using a virtual beam-splitter network was obtained experimentally [13], but there are reports on entanglement experimentally generated by an OPO that are limited to two spatial modes [14,15]. Recently, Patera *et al.* [16] theoretically demonstrated that multimode OPOs can produce a great variety of multipartite CV entangled states through appropriate control of the parametric interaction.

Recently, we have simultaneously produced two pairs of entangled Hermite–Gauss modes with a type II OPO and demonstrated that the entanglement is a CV hyperentanglement with a type II OPO [17]. In this report, we used the $HG_{02}^{45^\circ}$ mode pump to control the parametric nonlinear interaction and directly produce spatial quadripartite CV entanglement among first-order Hermite–Gaussian modes in a type II OPO below the threshold. We also realized spatial nonlocal separation and measurement in four modes. To our knowledge, this is the first time that spatially separable CV quadripartite entanglement has been demonstrated with the same frequency by an OPO, which is beneficial for coherent manipulation. The experimental system is scalable to higher-dimensional spatial modes by changing the spatial profile of the pump beam. Entanglement will be a promising source for future spatial multichannel quantum information.

In principle, we used the characteristics of the spatial freedom of light to generate quadripartite entanglement. In our model, shown in Fig. 1, the spatially tailored pump beam with a frequency of 2ω drives a type II crystal in an optical cavity and quadripartite entanglement with frequency ω is generated from the cavity. The entanglement is in first-order Hermite–Gaussian (HG) modes with the same "family index" ($f = 1$) [18] (which are degenerate modes in the cavity): HG_{01}^{i}, HG_{01}^{s}, HG_{10}^{i}, and HG_{10}^{s}, where i (idle) and s (signal) are the polarizations of the beams. In the interaction picture, assuming perfect phase

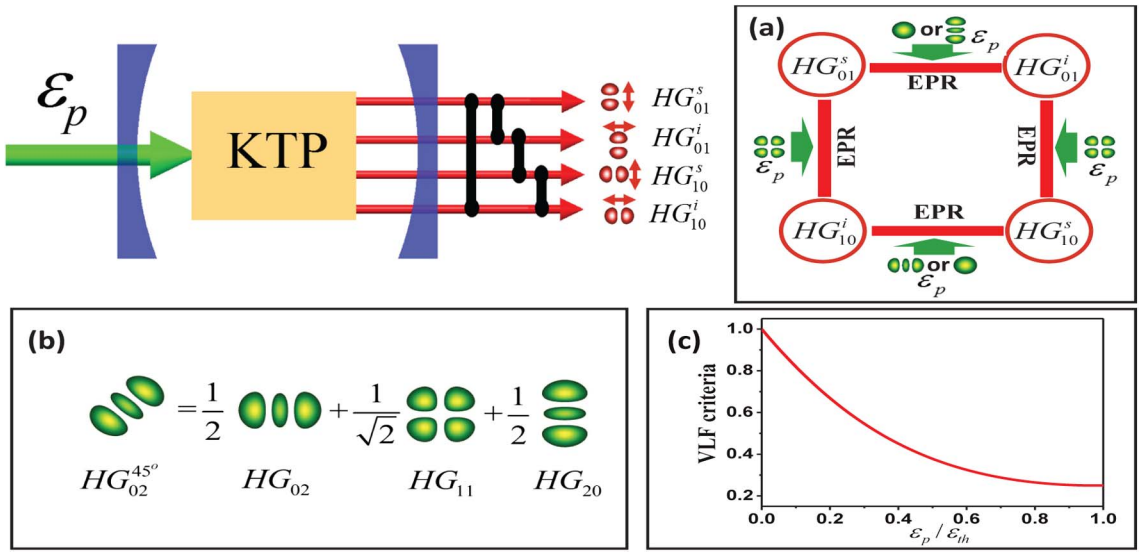

Fig. 1. Schematic illustration of the physical system. The spatially tailored pump beam ε_p (green) drives an OPO with a type II nonlinear crystal (KTP) below threshold, and spatial quadripartite entanglement among four first-order HG modes (red) with different polarizations (i, s) is generated. (a) Relationship between the spatial mode of the pump field ε_p (green) and the spatial modes of entangled down-conversion fields (red). EPR (red thick line) represents the entanglement between a pair of down-conversion fields with HG modes. (b) Spatial distribution for pump mode $HG_{02}^{45^\circ}$ used in the experiment, which is superposition of three types of HG modes. (c) Theoretical solution for VLF criteria below the OPO threshold.

matching and exact resonance between the field and the cavity and assuming that the pump is not depleted, the interaction Hamiltonian of the system is

$$H_{\text{int}} = i\hbar\varepsilon_p \sum_{j,k} \kappa_{kj} \hat{a}_k^{i\dagger} \hat{a}_j^{s\dagger} + \text{h.c.} \tag{1}$$

Here, $\hat{a}_k^i$ and $\hat{a}_j^s$ are annihilation operators describing the intracavity fundamental fields. k and $j = 01, 10$ denote the types of HG mode and i and s denote the polarizations of the HG mode. ε_p is the average amplitude of the pump field. κ_{kj} is the nonlinear coupling constant [18], which is dependent on the spatial overlap between the pump and down-conversion fields.

The dynamics of the intracavity fields are then given by the quantum Langevin equations [15]:

$$\begin{aligned} \frac{d\hat{a}_k^i}{dt} &= -\gamma \hat{a}_k^i + \varepsilon_p \sum_j \kappa_{kj} \hat{a}_j^{s\dagger} + \sqrt{2\gamma}\hat{a}_{kc}^i, \\ \frac{d\hat{a}_j^s}{dt} &= -\gamma \hat{a}_j^s + \varepsilon_p \sum_k \kappa_{kj} \hat{a}_k^{i\dagger} + \sqrt{2\gamma}\hat{a}_{jc}^s, \end{aligned} \tag{2}$$

where γ is the cavity loss rate (assumed to be identical for all modes) and $\hat{a}_{kc}^s$ and $\hat{a}_{jc}^s$ are the annihilation operators for vacuum fields.

It follows from the definition of κ_{kj} that the relationship between the spatial mode of the pump field (green) and the spatial modes of the entangled down-conversion fields (red) are shown in Fig. 1(a). To generate the entanglement (EPR) between the HG_{01}^i and HG_{01}^s down-conversion fields, the spatial profiles of the pump beam must be in HG_{00} or HG_{02} modes; for the entanglement between HG_{10}^i and HG_{10}^s, the pump beam must be in HG_{00} or HG_{20} modes. Moreover, to generate entanglement between HG_{01}^i and HG_{10}^s or entanglement between HG_{10}^i and HG_{01}^s, the spatial profile of the pump beam is only HG_{11} mode. Thus, to obtain spatial quadripartite CV entanglement among first-order Hermite–Gaussian (HG) modes (HG_{01}^i, HG_{01}^s, HG_{10}^i, and HG_{10}^s), the effective spatial pump beam must be a coherent superposition of HG_{11}, HG_{02}, and HG_{20} or a superposition of HG_{11} and HG_{00}. It is complex to experimentally generate the hybrid mode through coherent superposition of different spatial modes on beam splitters. Fortunately, $HG_{02}^{45^\circ}$, which is equal to the superposition of HG_{11}, HG_{02}, and HG_{20}, is an effective and simple pump mode used to generate quadripartite entanglement among HG modes, as shown in Fig. 1(b).

With the $HG_{02}^{45^\circ}$ pump, $\kappa_{kj} = \frac{\chi_0}{2\sqrt{2}}$ is identical for all down-conversion fields. χ_0 is the nonlinear coupling constant between the HG_{00} pump and the HG_{00} down-conversion fields. The Hamiltonian has the same form as quadripartite entanglement of the optical frequency comb in Ref. [8]. As shown in Fig. 1(c), below the OPO threshold, the van Loock-Furusawa (VLF) CV multipartite entanglement criteria [19] are violated, demonstrating quadripartite entanglement. The largest violation, and thus the maximum quadripartite entanglement, is near the threshold $|\varepsilon_{\text{th}}|^2$, which is twice the threshold of a standard HG_{00} mode OPO.

The experimental setup is depicted in Fig. 2. We used a high-power CW solid-state laser as the laser source, which delivers light with wavelengths of 1080 and 540 nm. The 1080-nm light was transmitted through a three-mirror ring cavity (RC), which tailors the spatial profile of the beam into the HG_{10} mode, and was then injected into the OPO as the seed with a power of 3 mW and a polarization of 45°. The 540-nm beam was tailored by the RC into the HG_{20} mode and rotated to $HG_{02}^{45^\circ}$ by a Dove prism (MR), which then drives the OPO as the pump. The OPO cavity included two mirrors with a radius of curvature of 30 mm (M1 and M2 in Fig. 2). The piezo-actuated mirror, M1, was used as the input coupler (with a high reflectivity at 540 and 1080 nm), and mirror M2 was the output coupler of the entangled beams at 1080 nm (with a

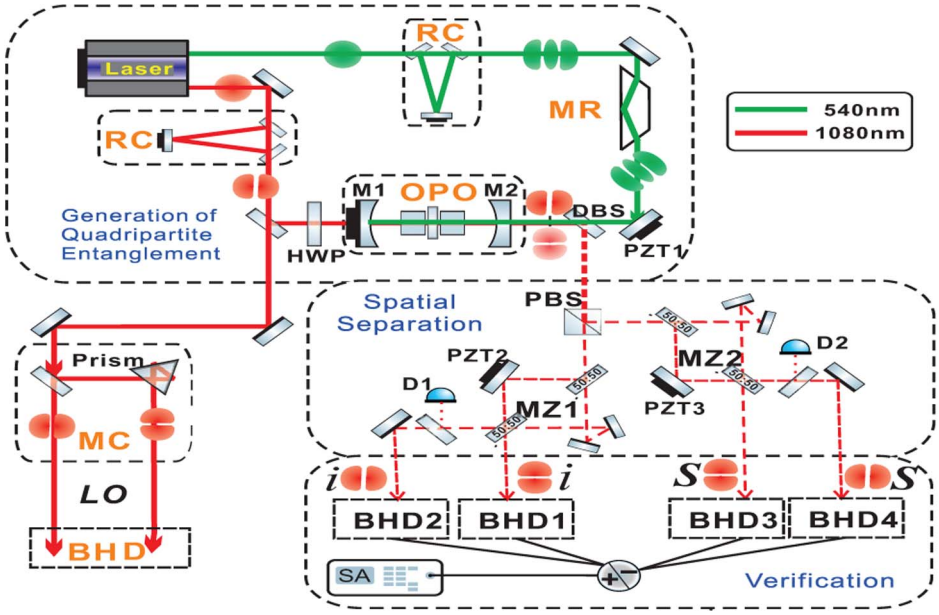

Fig. 2. Experimental setup. The quadripartite entanglement is generated by a type II OPO, and then it is separated into four nonlocal parts using two asymmetric Mach–Zehnder interferometers (MZ1 and MZ2) and verified by four sets of balanced homodyne detectors (BHD). RC, three-mirror-ring cavity for generation of HG mode; MR, mode rotator; DBS, dichroic beam splitter; PBS, polarizing beam splitter; HWP, half-wave plate; PZT, piezoelectric element for controlling phase; LO, local oscillator; MC, mode converter for generation of LO of the HG_{01} mode from the HG_{10} mode; D1 and D2, detectors; and SA, spectrum analyzer.

transmission of 4.1% at 1080 nm and an antireflective coating for 540 nm). A device for astigmatism compensation [17] was placed into the cavity to achieve simultaneous resonation of the four modes (HG^{i}_{01}, HG^{s}_{01}, HG^{i}_{10} and HG^{s}_{10}) in the cavity.

In our setup, the OPO threshold of the HG_{00} mode is 400 mW. With the 540 mW $HG^{45^\circ}_{02}$ pump that is below the OPO threshold of the first-order HG mode, spatial quadripartite CV entanglement can be generated when the relative phase between the pump field and the injected signal is locked in a state of deamplification with PZT1. Using a dichroic beam splitter (DBS), entanglement was separated from the pump. The power of the entanglement was 25 μW.

The output of the entangled beams was divided by a polarizing beam splitter (PBS) into two parts (i and s) with orthogonal polarization. Each part includes both HG_{01} and HG_{10} modes. The two arms of the asymmetric Mach–Zehnder interferometers (MZ1 and MZ2) [20] have odd and even numbers of reflectors, respectively. Because of the different interference conditions for the HG_{01} and HG_{10} modes through asymmetric Mach–Zehnder interferometers, HG_{01} and HG_{10} modes were separated and independently output from the two ports. In the experiment, both MZ1 and MZ2 have transmissions of 98%. Detectors D1 and D2 provide a control signal for locking PZT2 and PZT3 of the Mach–Zehnder. As the result, the quadripartite entanglement is separated into four nonlocal parts: HG^{i}_{01} (mode 1), HG^{i}_{10} (mode 2), HG^{s}_{01} (mode 3), and HG^{s}_{10} (mode 4). Then, the quadripartite entanglement was verified by four sets of balanced homodyne detectors (BHD1–BHD4) with spatially tailored local oscillators (LOs) using a mode converter (MC). The LO beam was either in the HG_{10} or HG_{01} mode, depending on which spatial mode was measured. The measured correlation variances were then analyzed with a spectrum analyzer (SA). The measured efficiency of the spatial overlaps between the signal and the LO in the homodyne detector for balanced homodyne detectors (BHD) 1, 2, 3, and 4 were 92%, 93%, 92%, and 93%, respectively, and the measured photodiode (FND-500) efficiency was 92%.

The correlation variances were obtained by joint BHD according to the VLF criteria at an analysis frequency of 6 MHz. As shown in Fig. 3, the trace (1) is the shot-noise limit (SNL) and the trace (2) is the correlation variance normalized to SNL. $\langle(\delta P^{i}_{01} - \delta P^{s}_{01})^2\rangle$, $\langle(\delta P^{s}_{01} - \delta P^{i}_{10})^2\rangle$, $\langle(\delta P^{i}_{10} - \delta P^{s}_{10})^2\rangle$, $\langle(\delta P^{s}_{10} - \delta P^{i}_{01})^2\rangle$, and $\langle(\delta X^{i}_{01} + \delta X^{s}_{01} + \delta X^{i}_{10} + \delta X^{s}_{10})^2\rangle$ are 1.02 ± 0.18 dB, 0.89 ± 0.21 dB, 1.12 ± 0.21 dB, 0.68 ± 0.20 dB, and 1.44 ± 0.20 dB below the SNL, respectively. Here, $X = (\hat{a} + \hat{a}^{\dagger})/2$ is the amplitude quadrature and $P = (\hat{a} - \hat{a}^{\dagger})/2i$ is the phase quadrature. According to the VLF criteria for quadripartite GHZ CV entanglement,

$$
\begin{aligned}
S1 &= \langle(\delta P^{i}_{01} - \delta P^{s}_{01})^2\rangle + \langle(\delta X^{i}_{01} + \delta X^{s}_{01} + g_1 \delta X^{i}_{10} + g_2 \delta X^{s}_{10})^2\rangle \\
&= 0.76 \pm 0.03 < 1, \\
S2 &= \langle(\delta P^{s}_{01} - \delta P^{i}_{10})^2\rangle + \langle(g_3 \delta X^{i}_{01} + \delta X^{s}_{01} + \delta X^{i}_{10} + g_4 \delta X^{s}_{10})^2\rangle \\
&= 0.77 \pm 0.04 < 1, \\
S3 &= \langle(\delta P^{i}_{10} - \delta P^{s}_{10})^2\rangle + \langle(g_5 \delta X^{i}_{01} + g_6 \delta X^{s}_{01} + \delta X^{i}_{10} + \delta X^{s}_{10})^2\rangle \\
&= 0.75 \pm 0.04 < 1, \\
S4 &= \langle(\delta P^{s}_{10} - \delta P^{i}_{01})^2\rangle + \langle(\delta X^{i}_{01} + g_7 \delta X^{s}_{01} + g_8 \delta X^{i}_{10} + \delta X^{s}_{10})^2\rangle \\
&= 0.79 \pm 0.03 < 1.
\end{aligned}
\tag{3}
$$

All of the inequalities in Eq. (3) are satisfied, and the quadripartite GHZ entanglement among the four spatial modes was thus demonstrated experimentally. $g_i (i = 1, 2, \ldots, 8)$ are arbitrary real parameters that were used to optimize the violation of

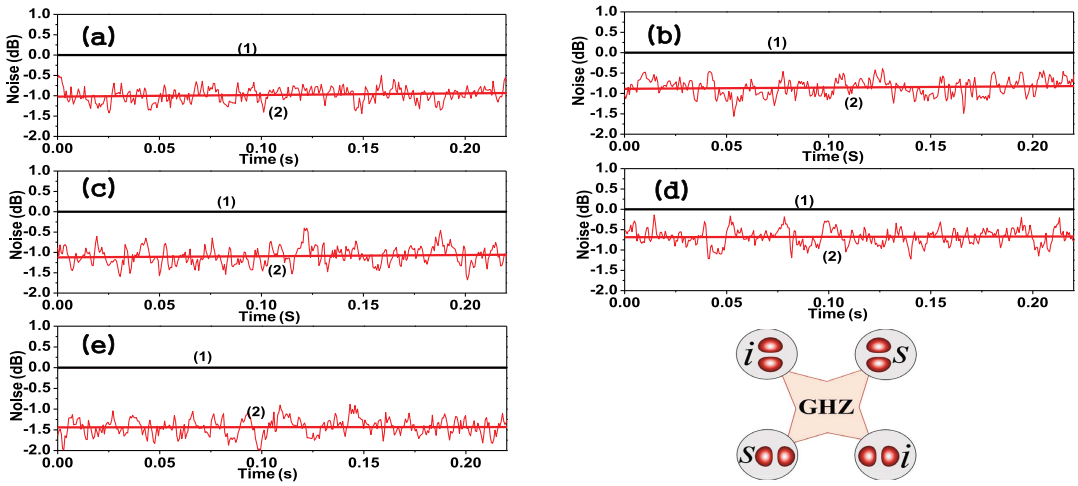

Fig. 3. Results of spatial quadripartite GHZ entanglement. (a) $\langle(\delta P^i_{01} - \delta P^s_{01})^2\rangle$, (b) $\langle(\delta P^s_{01} - \delta P^i_{10})^2\rangle$, (c) $\langle(\delta P^i_{10} - \delta P^s_{10})^2\rangle$, (d) $\langle(\delta P^s_{10} - \delta P^i_{01})^2\rangle$, and (e) $\langle(\delta X^i_{01} + \delta X^s_{01} + \delta X^i_{10} + \delta X^i_{10})^2\rangle$. Trace (1) is the SNL and trace (2) is the correlation variance normalized to SNL. The measured parameters of SA are a resolution bandwidth of 1 MHz and a video bandwidth of 100 Hz.

these inequalities. In this experiment, $g_i = 1$, which is not optimal [19] but is sufficient to verify the existence of quadripartite GHZ entanglement.

In the experiment, there are factors that degrade the correlation. One major factor is the various loss of our setup, including the cavity loss and a total measurement loss owing to propagation loss and BHD and Mach–Zehnder interferometer inefficiencies. Another main factor is the intensity imbalance between HG_{01} and HG_{10} modes, because only an HG_{10} seed affects the correlation between HG_{01} and HG_{10} modes. Also, the optimum pump power was not reached in the experiment and the purity of the pump spatial profile needs to be further improved. The entanglement can be improved by optimizing the experimental setup to meet the needs of particular applications.

We experimentally demonstrated spatial quadripartite GHZ CV entanglement. The presented experimental system can also be used to generate spatial cluster entanglement and be expanded to higher-dimensional entanglement. The presented experimental system and scheme pave an efficient way to generate spatial multimode CV entanglement, which would improve the quality of an image in quantum imaging [21] and has advantages in terms of the complexity of protocols [10,22] to expand quantum channels. Another promising application is to build an interface between light and atoms and to hopefully generate multi-system CV entanglement of atoms [23–25].

Funding. Ministry of Science and Technology of the People's Republic of China (MOST) (2016YFA0301404); NSFC Project for Excellent Research Team (61121064); National Natural Science Foundation of China (NSFC) (11274212, 61405108, 91536222); University Science and Technology Innovation Project in Shanxi Province (2015103).

REFERENCES

1. A. Einstein, B. Podolsky, and N. Rosen, Phys. Rev. **31**, 553 (1935).
2. S. L. Braunstein and P. van Loock, Rev. Mod. Phys. **77**, 513 (2005).
3. J. W. Pan, Z. B. Chen, C. Y. Lu, H. Weinfurter, A. Zeilinger, and M. Zukowski, Rev. Mod. Phys. **84**, 777 (2012).
4. P. van Loock and S. L. Braunstein, Phys. Rev. Lett. **84**, 3482 (2000).
5. X. C. Yao, T. X. Wang, P. Xu, H. Lu, G. S. Pan, X. H. Bao, C. Z. Peng, C. Y. Lu, Y. A. Chen, and J. W. Pan, Nat. Photonics **6**, 225 (2012).
6. X. Su, Y. Zhao, S. Hao, X. Jia, C. Xie, and K. Peng, Opt. Lett. **37**, 5178 (2012).
7. J. Roslund, R. M. de Arajo, S. Jiang, C. Fabre, and N. Treps, Nat. Photonics **8**, 109 (2013).
8. M. Chen, N. C. Menicucci, and O. Pfister, Phys. Rev. Lett. **112**, 120505 (2013).
9. S. Yokoyama, R. Ukai, S. C. Armstrong, C. Sornphiphatphong, T. Kaji, S. Suzuki, J. Yoshikawa, H. Yonezawa, N. C. Menicucci, and A. Furusawa, Nat. Photonics **7**, 982 (2013).
10. M. Lassen, V. Delaubert, J. Janousek, K. Wagner, H. A. Bachor, P. K. Lam, N. Treps, P. Buchhave, C. Fabre, and C. C. Harb, Phys. Rev. Lett. **98**, 083602 (2007).
11. K. Wagner, J. Janousek, V. Delaubert, H. Zou, C. Harb, N. Treps, J. F. Morizur, P. K. Lam, and H. A. Bachor, Science **321**, 541 (2008).
12. N. Treps, N. Grosse, W. P. Bowen, C. Fabre, H. A. Bachor, and P. K. Lam, Science **301**, 940 (2003).
13. S. Armstrong, J. F. Morizur, J. Janousek, B. Hage, N. Treps, P. K. Lam, and H. A. Bachor, Nat. Commun. **3**, 1026 (2009).
14. M. Lassen, G. Leuchs, and U. L. Andersen, Phys. Rev. Lett. **102**, 163602 (2009).
15. J. Janousek, K. Wagner, J. F. Morizur, N. Treps, P. K. Lam, C. C. Harb, and H. A. Bachor, Nat. Photonics **3**, 399 (2009).
16. G. Patera, C. Navarrete-Benlloch, G. J. De Valcárcel, and C. Fabre, Eur. Phys. J. D **66**, 241 (2012).
17. K. Liu, J. Guo, C. X. Cai, S. F. Guo, and J. R. Gao, Phys. Rev. Lett. **113**, 170501 (2014).
18. C. Navarrete-Benlloch, G. J. De Valcárcel, and E. Roldán, Phys. Rev. A **79**, 043820 (2009).
19. P. van Loock and A. Furusawa, Phys. Rev. A **67**, 052315 (2003).
20. V. Delaubert, N. Treps, C. C. Harb, P. K. Lam, and H. A. Bachor, Opt. Lett. **31**, 1537 (2006).
21. N. Treps, U. Andersen, B. Buchler, P. K. Lam, A. Maître, H. A. Bachor, and C. Fabre, Phys. Rev. Lett. **88**, 203601 (2002).
22. C. M. Caves and P. D. Drummond, Phys. Rev. Lett. **66**, 481 (1994).
23. R. Inoue, T. Yonehara, Y. Miyamoto, M. Koashi, and M. Kozuma, Phys. Rev. Lett. **103**, 110503 (2009).
24. A. Picón, A. Benseny, J. Mompart, J. R. De Vázquez Aldana, L. Plaja, G. F. Calvo, and L. Roso, New J. Phys. **12**, 083053 (2010).
25. C. Gross, H. Strobel, E. Nicklas, T. Zibold, N. Bar-Gill, G. Kurizki, and M. K. Oberthaler, Nature **480**, 219 (2011).